The Boundary Condition of a 3D Continuum Model for a Quasi 2D Plane Strain Condition

S. Chaiyaput[1] and M. Sugimoto[2]
[1]*Department of Civil Engineering, School of Engineering, King Mongkut's Institute of Technology Ladkrabang, Bangkok 10520, Thailand*
[2]*Department of Civil and Environmental Engineering, Nagaoka University of Technology, Nagaoka, Niigata, Japan*
E-mail: salisa.fern@gmail.com; salisa.ch@kmitl.ac.th

ABSTRACT: The half-model has been used in the finite element analysis, based on the symmetric condition against the tunnel's longitudinal, vertical plane, but this design concept cannot apply to a staggered lining. Therefore, the authors have proposed a multi-ring model to present the segmental lining behavior of a 3D continuum ground model in the case of staggered building, but the proposed 12-ring model shows the different axial force distributions in circumferential directions between the center of the model and the end of the model, especially in cases of soft soil. Accordingly, to make clear, the mechanism of the above difference and to establish the analysis condition of the proposed model for quasi 2D plane strain condition, this paper evaluates the influence of boundary condition on the transverse cross section at the end of the segmental lining on the segmental lining behavior, based on the analyzed axial force and bending moment in soft and stiff ground conditions using both the 2-ring model and a 12-ring model. As a result, it was confirmed that the proposed 2-ring model could simulate the segmental lining behavior under quasi 2D plane strain condition.

KEYWORDS: Segmental lining, Staggered arrangement, Continuum ground model, 3D FEM, Boundary condition.

1. INTRODUCTION

One of the major problems of underground construction is ground deformation, which is challenging for engineers. The design of a tunnel lining requires accurate results for a good engineering design and a clear understanding of a complicated problems. Therefore, the many design methods which have been continuously proposed ranging from the basic formula to the advanced finite element analysis. In particular, the finite element model has been continuously developed to simulate the lining behavior. Especially, the three-dimensional finite element model (3D FEM model) has been used to simulate construction projects in details, using actual situations, such as material properties, soil properties, machine control, acting loads, and the characteristics of the interaction between the lining and the excavation surface. These factors are important for the calculation processed in order to increase model efficiency. To save calculation time and cost, the 3D FEM model commonly used the half-model of the tunnel dimension based on the symmetric condition against the tunnel's longitudinal vertical planes (e.g., Gnilsen, 1989). Generally, the half-model was adopted to simulate the tunnel behavior in cases of NATM, which is suitable for construction in hard rock (e.g., Dasari et al., 1996; Sharma., 2000; Yeo et al., 2009). While, the shield tunneling method is suitable for construction in soil and soft rock, where the segmental lining is adopted as support system to protect the ground movement. The segmental lining is not a continuous structure because of the existence of joints in the longitudinal and circumferential directions relative to connect segments. The longitudinal joints and circumferential joints significantly affect the lining behavior (Muir Wood, 1975; Koyama, 2003; Klappers et al., 2006; Lu et al., 2006; Teachavorasinskun and Chubuppakarn, 2010; Huang et al., 2012, and Li et al., 2013). Moreover, since in case of staggered building, the longitudinal joints are, by turn, for odd number rings and even number rings. Therefore, the half-model cannot be used for the segmental lining model. The transferred bending moment to neighbored ring, in the case of staggered building, is shown in Figure 1.

With regard to the 3D FEM continuum ground model in [the] case of staggered lining, Chaiyaput and Sugimoto (2016) proposed the multi-ring model by considering the effect of boundary conditions of segmental lining model upon its sectional force. When the proposed model satisfies a quasi 2D plane strain condition, the axial force distributions in circumferential direction should be the same at any position. But as shown in Figure 2, the axial force at the center of the model ("12rings R7": Ring No. 7 of the 12-ring model) is different from that at the end of the model ("2rings R1" and "12 rings R1": Ring No. 1 of the 2-ring model and the 12-ring model, respectively) in the cases of oft ground.

To overcome the abovementioned problem, this paper investigated the mechanism of boundary effect on the transverse cross section at the end of the model on the sectional force, using the proposed 3D FEM continuum ground model.

2. 3D FEM CONTINUUM MODEL

2.1 Finite Element Model

The proposed 3-D FEM model represents a realistic condition in the construction site by setting the interaction between the lining and the ground and the sequences of the construction process without any significant changes. The tunnel lining 3D finite element model consists of three components, which are ground model, interaction model and lining model, as shown in Figure 3. The 3D curve shell element with four nodes was utilized for modeling the lining model. The

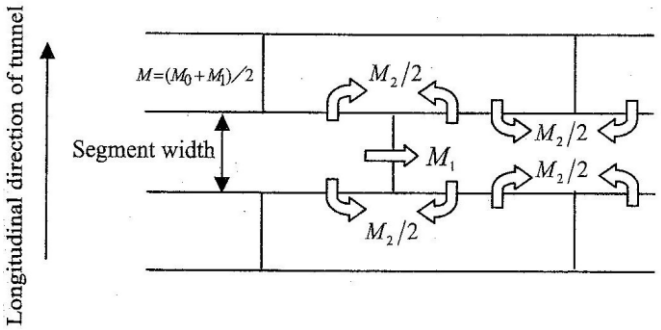

$M = M_1 + M_2$
$M_0 = M + M_2 = (1 + \zeta)M$
$M_1 = M - M_2 = (1 - \zeta)M$

where,

M	: Bending moment calculated in a ring with uniform flexural rigidity, ηEI
M_0	: Design bending moment for main section
M_1	: Design bending moment for segment joint
η	: decreasement rate of EI
ζ	: Increment rate of M

Figure 1 Transferred bending moment to adjacent rings (JSCE, 2006)

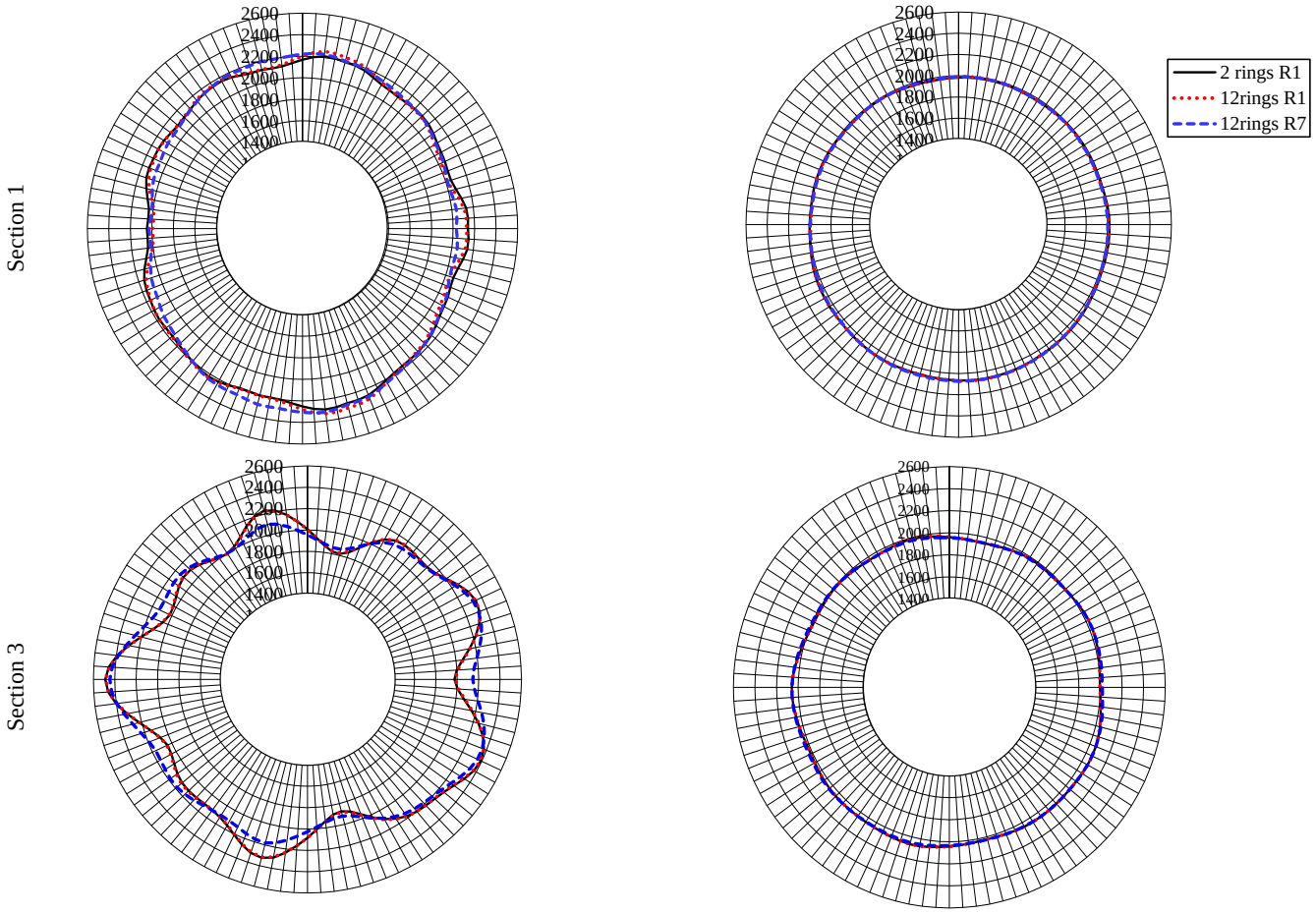

(a) k_n = 10 MN/ m^3 (b) k_n = 100 MN/ m^3

Figure 2 Axial force in the circumferential direction at each section. (kN/m) (Chaiyaput and Sugimoto, 2016)

solid element with eight nodes was applied to represent the geometry of the ground model. In addition, the tunnel lining is composed of segmental rings in longitudinal and circumferential orientations. The connection points were connected by tying between the two nodes of the model. The connection joints were divided into three types of the spring model, which are rotation spring, shear spring, and touching spring to simulate the behavior of longitudinal joints, circumferential joints, and surrounding ground, respectively. The rotation spring and shear spring were connected by two nodes, which were assigned in the same coordinates. The characteristic of rotation spring and shear spring as detailed in Figure 4(a).

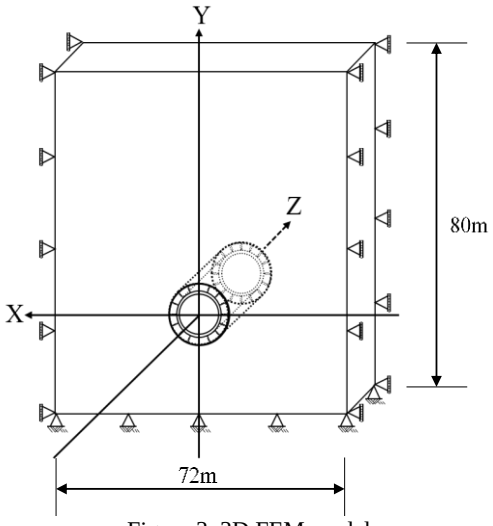

Figure 3 3D FEM model

While, touching spring was the connection between the surface of segmental lining and the surfacee of initial excavation to simulate the the acting earth pressure on the segmental lining. Here the touching spring has a characteristics as shown in Figure 4(b) so that the acting earth pressure on the segmental lining without the displacement of the excavation surface is the earth pressure at rest; and the acting earth pressure on the segmental lining is non-tension.

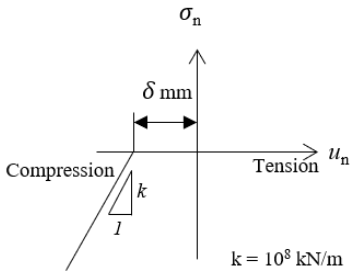

(a) rotation spring and shear spring

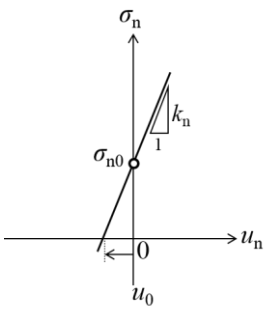

(b) touching spring

Figure 4 Characteristics of spring model

2.2 Boundary Conditions

Figure 5 shows the used boundary conditions of the segmental lining on the transverse cross section at the tunnel end in the 3-D FEM model. Figure 5(a) BC1 shows the ordinary boundary condition which fixes the displacement in the tunnel's axis direction only (Chaiyaput and Sugimoto, 2016). Figure 5(b) BC2 shows the new boundary condition which allows for rotation around the tunnel axis only, so that the segments are perpendicular to the transverse cross section at the tunnel end, with BC1 condition. To ensure the 2D plane strain condition, these boundary conditions were also applied to the ground on the transverse cross section at the tunnel end. The vertical roller was used on the both sides of the model, along the longitudinal direction. Moreover, the fixed boundary conditions were adopted at the bottom of the model to fix both horizontal and vertical displacements. In contrast, the free boundary condition was used at the top of the model.

2.3 Sequential Analysis

The calculation procedure was divided into two phases, that is; the initial stress analysis, and the tunnel excavation and the segment lining installation as follows, as illustrated in Figure 6:

1) Initial stress analysis: Before excavation, the self-weight of the ground is loaded to generate earth pressure at rest was as illustrated in Figure 6(a).
2) Tunnel excavation and installation of the segmental lining: The soil inside the tunnel is deactivated. To simulate the characteristics of the touching spring in Figure 4(b), the enforced displacement $u_{0,}$ as shown in Figure 4(b), is applied to the excavation surface in the normal direction. The 3-D shell beam model and the touching spring between the ground and the lining are installed. After that, the fixation on the excavation surface is released. This is "The analysis phase" as illustrated in Figure 6(b).

3. ANALYSIS CONDITIONS

3.1 Analysis Parameters

Table 1 shows the properties of the segmental lining and the ground conditions for the analysis, which were set based on actual site data (Sugimoto et al., 2011). The concrete segmental ring has a diameter of 7.87 m, segmental width of 1.00 m, and thickness of 0.37 m. Figure 7 shows the position of the longitudinal joints and circumferential joints in odd number rings and even number rings. The ground was assumed to be one homogeneous layer to simplify the model, since this paper aims to discuss the effect of boundary condition on the sectional force. The analysis model dimension was 72 m in width and 80 m in depth, where the depth under the tunnel is 30.642 m, which is equivalent to about 4 times the tunnel diameter.

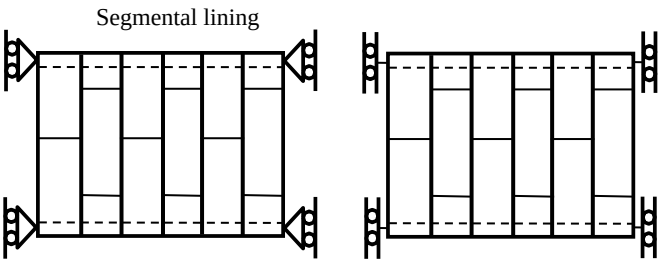

(a) BC1 (b) BC2

Figure 5 Boundary conditions at tunnel end

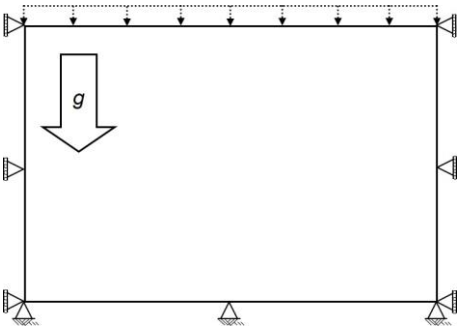

(a) initial stress analysis

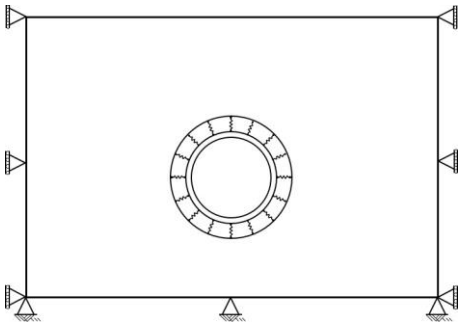

(b) the tunnel excavation and the segment lining installation

Figure 6 Sequential analysis

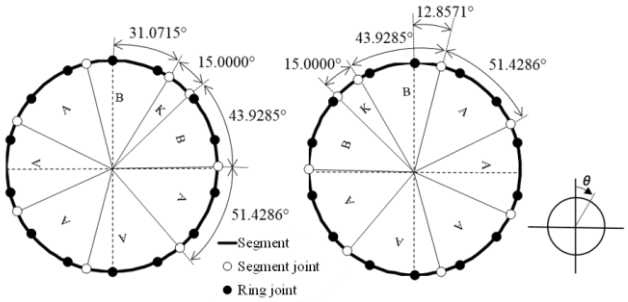

(a) odd number rings (b) even number rings

Figure 7 Positions of segmental joints (longitudinal joint) and ring joints (circumferential joint)

Table 1 Properties of the segment lining and the ground condition

Component	Value
Segment	
Radius (m)	3.935
Width (m)	1.000
Height (m)	0.370
Young's modulus (GN/m^2)	33
Poisson's ratio	0.2
Density (kN/m^3)	28.0
Joints	
Segment J. spring const. (MN-m/rad/m)	42.5
Ring J. radial spring const. (MN/m/m)	478
Ring J. tangential spring const. (MN/m/m)	1050
Ring J. axial spring const. (MN/m/m)	173
Ground	
Overburden depth (m)	41.488
Ground water level (m)	GL-11.408
Submerged density (kN/m^3)	5.5
Water density (kN/m^3)	10.0
Coef. of earth pressure at rest K_{H0}	0.5
Coef. of ground reaction k_H (MN/m^3)	10, 100
k_V (MN/m^3)	10, 100
k_t (MN/m^3)	0.001
Touching radial spring const. (MN/m/m)	6181
Touching tangential spring const. (kN/m/m)	0.618

Table 2 Analysis cases

Case	BC	No. of ring	k_n (MN/m^3)
111	BC 1	12 rings	10
112		12 rings	100
121		2 rings	10
122		2 rings	100
211	BC 2	12 rings	10
212		12 rings	100
221		2 rings	10
222		2 rings	100

To investigate the effect of ground conditions on the sectional force and lining behavior, the coefficient of subgrade reaction, k_n, was considered as a parameter. From the view point of the ground where shield tunneling methods can be applied, the grounds with k_n = 10 MN/m^3 and 100 MN/m^3 are called "soft ground" and "stiff ground", respectively in this paper (JSCE, 2006). Young's modulus of ground in the FEM model, E, was obtained from the coefficient of subgrade reaction, k_n, using the following empirical equation (RTRI, 2002):

$$k_n = 1.58\alpha E B_v^{-0.75} \quad (1)$$

$$B_v = 2R_c \quad (2)$$

where α is the factor for the test method of E, B_v is the equivalent diameter of the tunnel, and R_c is the radius of the tunnel.

3.2 Lining Model

In this model, the segmental lining and excavation surface were divided into 100 elements in the circumferential direction in each ring. Moreover, the segmental lining widths of 1 m were divided by four, that is, the interval of the node is 0.25 m, as shown in Figure 8. As a ring model consists of four shell elements in width, Sec. 1 and Sec. 3 are the cross-sections at the end and the center of the rings, respectively. Sec. 2 is that at the middle between Sec. 1 and Sec. 3. For staggered building of segmental lining, the sectional force of segmental lining (i.e., the axial force in the circumferential direction and the bending moment around the tunnel axis) is considered to be affected by the boundary conditions at the tunnel end of the model, since the bending moment around the tunnel axis transfers not only in the circumferential joints but also in the longitudinal joints as shown in Figure 1. Therefore, the influence of the joints under staggered lining was examined by the sectional force of segmental ring. To investigate the effect of boundary conditions at the tunnel end on the sectional force in the case of staggered building, the boundary condition was considered as a parameter, that is, BC1 and BC2, as shown in Figure 5. The lining model with 2-ring and 12-ring are taken as an analysis parameter as shown in Table 2. Here, to ensure 2D quasi-plane strain condition, in other words, to eliminate the difference of the axial force of the segmental lining between at the end and center of the model, the segment was modelled by half a width at both ends of the lining model in 2-ring model and 12-ring model as shown in Figure 9. This is due to the distribution of the transferred sectional force of the segment lining through the circumferential joints should be symmetric against the cross section at the center of the segment ring under 2D quasi plane strain condition.

4. RESULTS AND DISCUSSIONS

4.1 Axial Force

To compare the axial force of the segmental lining in circumferential direction, N, at a different position, the maximum and minimum normalized difference rates of N, r_{Nmax} and r_{Nmin}, were defined as,

$$r_{Nmax} = \max\ (r_{Ni},\ i = 1\sim n)$$
$$r_{Nmin} = \min\ (r_{Ni},\ i = 1\sim n)$$

$$r_{Ni} = \frac{N_i - N_{0i}}{|N_0|_{max}} \quad (3)$$
$$|N_0|_{max} = \max\ (|N_{0i}|,\ i = 1\sim n)$$

where,

r_{Ni} : normalized difference rate of N at the node i
suffix 0 : standard value at a section
suffix i : node number in circumferential direction, and
n : no. of node in circumferential direction.

Here "standard value" is the N of Ring 7 of the 12 ring-model, which is expected to be under quasi 2-D plane strain conditions, since Ring 7 is at the center of the 12 ring-model and gets less influence of the boundary condition at the model end.

Figure 10 shows the r_{Nmax} and r_{Nmin} at the odd number rings of the 12 ring-model with k_n = 10 MN/m^3 and 100 MN/m^3 under the boundary conditions of BC1. From these figures, the followings were found:

1) In the case of the soft ground (k_n = 10 MN/m^3), the r_{Nmax} and r_{Nmin} at each section of the ring, except Ring 1, is close to 0, that is, the N distributions are almost same as those at each section of Ring 7, while the r_{Nmax} and r_{Nmin} is not close to 0, that is, the N distributions at each section of Ring 1 is different from those of Ring 7. Especially, the N distribution at Sec. 3 (the center section of the ring) of Ring 1 (the end ring) shows a maximum difference from those of Ring 7 (the center ring) with about 7% of the $|N_0|_{max}$. This indicates that the boundary conditions of BC1 give the influence to the N at the model end.

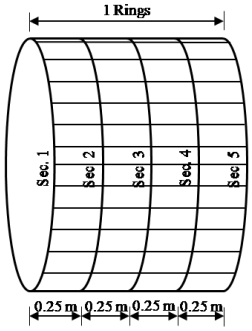

Figure 8 The interval of the nodes in a ring

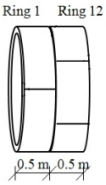

(a) 2 rings model

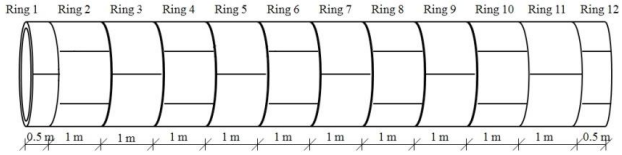

(b) 12 rings model

Figure 9 Segmental lining model (staggered building)

Table 3 Normalized difference rate of axial force in circumferential direction (%)

BC	k_n (MN/m^3)	Sec. no.	R1 (2rings) / R7 (12rings)		R1 (2rings) / R1 (12rings)		R2 (2rings) / R8 (12rings)		R2 (2rings) / R12 (12rings)	
			Min	Max	Min	Max	Min	Max	Min	Max
BC 1	10	Sec. 1	-4.41	3.56	-2.13	1.83	-4.41	3.56	-2.11	1.73
		Sec. 2	-0.94	0.94	-1.03	0.91	-0.93	0.94	-1.03	0.92
		Sec. 3	-5.85	6.95	-0.24	0.34	-5.85	6.95	-0.24	0.34
	100	Sec. 1	-0.77	0.48	-0.39	0.36	-0.77	0.51	-0.39	0.24
		Sec. 2	-0.12	0.12	-0.18	0.14	-0.12	0.11	-0.17	0.12
		Sec. 3	-0.75	1.08	-0.02	0.05	-0.75	1.08	-0.05	0.05
BC 2	10	Sec. 1	-0.16	0.14	-0.06	0.35	-0.16	0.16	-0.06	0.04
		Sec. 2	-0.04	0.04	-0.04	0.18	-0.04	0.04	-0.04	0.04
		Sec. 3	-0.20	0.22	-0.04	0.14	-0.20	0.22	-0.04	0.04
	100	Sec. 1	-0.05	0.05	-0.02	0.10	-0.05	0.05	-0.02	0.02
		Sec. 2	-0.02	0.04	-0.02	0.05	-0.02	0.04	-0.04	0.01
		Sec. 3	-0.05	0.05	-0.02	0.05	-0.05	0.05	-0.05	0.02

Example: "R1 (2rings)" is Ring1 of the 2 ring-model.
"/R7 (12rings)" is "normalized by the value at Ring7 of the 12 ring-model.

Table 4 Normalized difference rate of bending moment around tunnel axis (%)

BC	k_n (MN/m^3)	Sec. no.	R1 (2rings) / R7 (12rings)		R1 (2rings) / R1 (12rings)		R2 (2rings) / R8 (12rings)		R2 (2rings) / R12 (12rings)	
			Min	Max	Min	Max	Min	Max	Min	Max
BC 1	10	Sec. 1	-0.82	0.70	-0.13	0.23	-0.82	0.71	-0.12	0.11
		Sec. 2	-1.04	1.18	-0.85	0.40	-1.05	1.20	-0.31	0.40
		Sec. 3	-0.99	1.00	-0.58	0.35	-1.01	1.00	-0.28	0.35
	100	Sec. 1	-0.77	0.55	-0.14	0.38	-0.77	0.55	-0.15	0.11
		Sec. 2	-0.78	1.12	1.89	0.43	-0.80	1.12	-0.34	0.42
		Sec. 3	-0.73	1.01	-1.08	0.42	-0.75	1.01	-0.32	0.39
BC 2	10	Sec. 1	-0.11	0.09	-0.04	0.13	-0.11	0.10	-0.01	0.02
		Sec. 2	-0.25	0.29	-0.59	0.16	-0.27	0.29	-0.04	0.04
		Sec. 3	-1.04	0.89	-0.32	0.12	-1.04	1.00	-0.04	0.04
	100	Sec. 1	-0.10	0.07	-0.13	0.34	-0.10	0.08	-0.02	0.02
		Sec. 2	-0.20	0.28	-1.68	0.50	-0.21	0.28	-0.07	0.06
		Sec. 3	-1.00	0.72	-0.79	0.37	-1.02	0.80	-0.05	0.04

Example: "R1 (2rings)" is Ring1 of the 2 ring-model.
"/R7 (12rings)" is "normalized by the value at Ring7 of the 12 ring-model.

2) The N distributions in the stiff ground (k_n = 100 MN/m^3) shows the similar trend with those in the soft ground. But, the r_{Nmax} at Sec. 3 of Ring 1 is close to 1.0% of the $|N_0|_{max}$. This indicates that the boundary condition does not affect to the N distributions in stiff ground so much.

Figure 11 shows the r_{Nmax} and r_{Nmin} at the odd number rings of the 12 ring-model with k_n = 10 MN/m^3 and k_n = 100 MN/m^3 under BC2. From these figures, the following was found:

1) The r_{Nmax} and r_{Nmin} in all sections of all ring are close to 0%. This indicates the boundary condition BC2 can provide the N distribution under quasi 2D plane strain condition at any cross section of 12 ring-model.

Table 3 shows the maximum and minimum normalized different rate of the N at Ring 1 of the 2-ring model by the N at a specified Ring of the 12-ring model with k_n = 10 MN/m^3 and k_n = 100 MN/m^3 under BC1 and BC2. From this table, the following were found:

1) The r_{Nmax} and r_{Nmin} at "R1(2ring)/R7(12ring)", which represents the maximum change of the N at Ring 1 (the end ring) of the 2 ring-model as compared to Ring 7 (the center ring) of the 12 ring-model, show similar values with the r_{Nmax} and r_{Nmin} in Figure 10 and Figure 11, which represent the maximum change of N at Ring 1 (the end ring) from Ring 7 (the center ring) of the 12 ring-model, at any section for k_n = 10 MN/m^3 and k_n = 100 MN/m^3 under BC1 and BC2. This indicates that N at the end ring of the 2 ring-model is similar to that of the 12 ring-model.
2) In the case of BC1, the r_{Nmax} and r_{Nmin} at section 3 at "R1(2 ring)/R1(12 ring)", which represent the maximum change of the N at Ring 1 of the 2 ring-model from Ring 1 of the 12 ring-model, are close to zero for k_n = 10 MN/m^3 and 100 MN/m^3. This means that the N distribution at the model end section is almost same for the 2 ring-model and the 12 ring-model. While the r_{Nmax} and r_{Nmin} at section 1 at "R1(2ring)/R1(12ring)" is about 2% for k_n = 10 MN/m^3 and about 0.4% for k_n = 100 MN/m^3. This means that the N at section 1 (segment end along circumferential joints) of the 2 ring-model in soft soil gets more influence of BC1 than that of the 12 ring-model in stiff ground.
3) In the case of BC2, the r_{Nmax} and r_{Nmin} at "R1(2 ring)/R1(12 ring)" is close to zero at all section for k_n = 10 MN/m^3 and 100 MN/m^3. This means that the N distributions at each section are almost same irrespective of Ring Number. This indicates that BC2 can represent quasi 2D plane strain condition even using the 2 ring-model. This is because BC2 can generate the plane symmetric condition against the transverse cross section at the model end.
4) The above tendency at the odd number rings is similar at the even number rings.

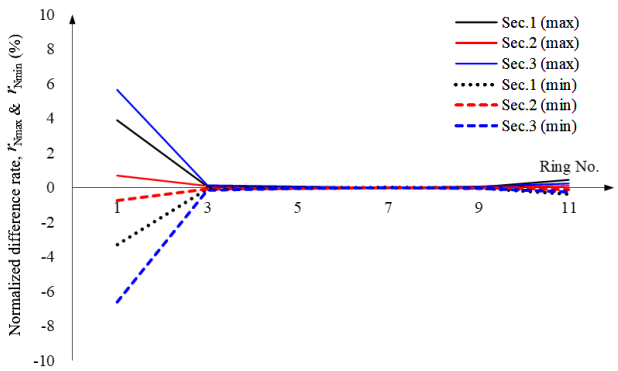

(a) k_n=10 MN/ m^3

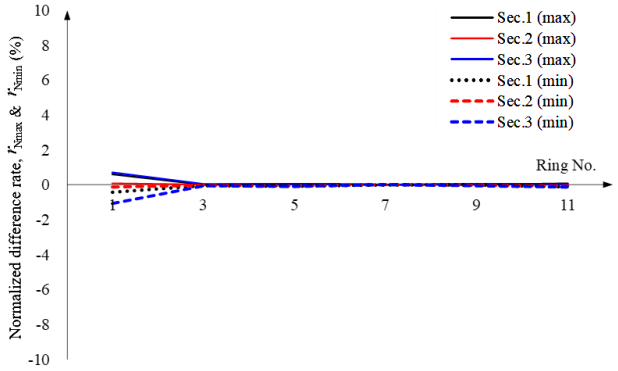

(b) k_n=100 MN/ m^3

Figure 10 Normalized difference rate of the axial force of 12 ring-model with BC1

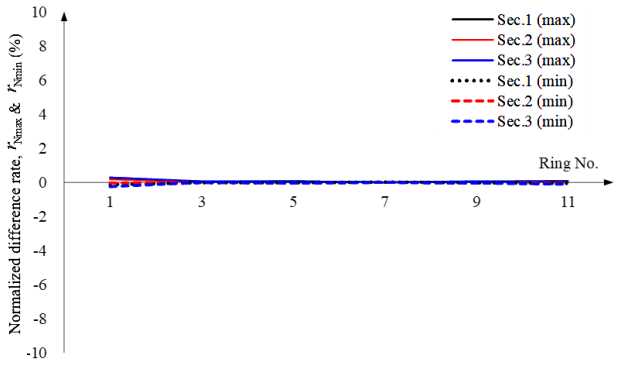

(a) k_n=10 MN/ m^3

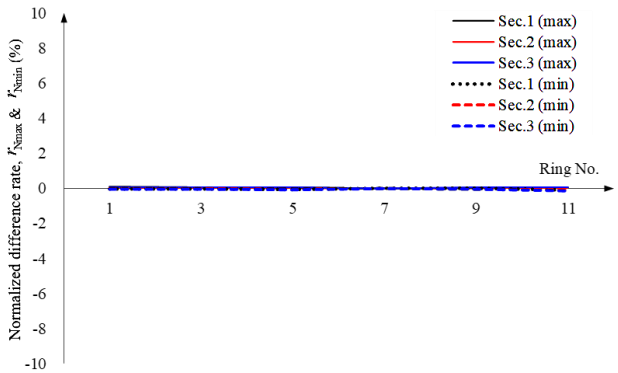

(b) k_n=100 MN/ m^3

Figure 11 Normalized difference rate of the axial force of 12 ring-model with BC2

4.2 Bending Moment

Figure 12 shows the calculated bending moment of the segmental lining around the tunnel axis, *M*, at Ring 1 of the 2-ring model and Ring 7 of the 12-ring model with k_n = 10 MN/m^3 and 100 MN/m^3 under BC1. Furthermore, Table 4 shows the maximum and minimum normalized difference rate of the *M*, $r_{M\,max}$ and $r_{M\,min}$, as shown in Eq. (4), at Ring 1 of the 2-ring model by the *M* at a specified Ring of the 12-ring model with k_n = 10 MN/m^3 and 100 MN/m^3 under BC1 and BC2.

$$
\begin{aligned}
r_{M\,max} &= \max\,(r_{Mi},\ i=1\sim n) \\
r_{M\,min} &= \min\,(r_{Mi},\ i=1\sim n) \\
r_{Mi} &= \frac{M_i - M_{0i}}{|M_0|_{max}} \\
|M_0|_{max} &= \max\,(|M_{0i}|,\ i=1\sim n)
\end{aligned}
\qquad (4)
$$

where,

r_{Mi} : normalized difference rate of *M* at the node i

From Figure 12 and Table 4 the following was found:

1) In the case of k_n = 10 MN/m^3, the *M* in Sec. 3 fluctuates more than the *M* in Sec. 1, since the *M* at the boundary between the two rings is levelled by the circumferential joints.
2) In the case of k_n = 100 MN/m^3, the *M* in stiff ground condition is almost close to 0 in each section. This is because the high ground reaction force due to the stiff ground limits the segment lining deformation.

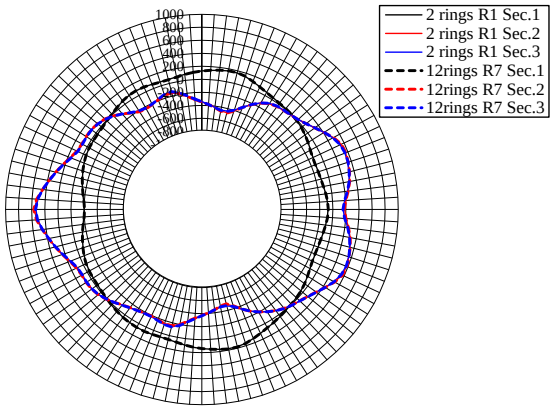

(a) k_n = 10 MN/ m^3

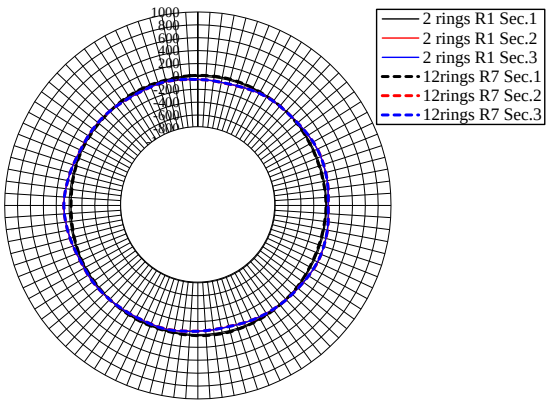

(b) k_n = 100 MN/ m^3

Figure 12 Bending moment around the tunnel axis. (BC1) (kN-m/m)

3) The $r_{\mathrm{M\,max}}$ and $r_{\mathrm{M\,min}}$ at "R1(2ring)/R7(12ring)", which represents the maximum change of the *M* at Ring 1 (the end ring) of the 2 ring-model from Ring 7 (the center ring) of the 12 ring-model, is less than 1% at any section for both soft and stiff ground conditions under BC1 and BC2. This indicates that the boundary conditions of the segmental lining at the model end do not produce a significant effect on the *M* for both ground conditions.
4) The $r_{\mathrm{M\,min}}$ at "R1(2ring)/R1(12ring)", which represents the maximum change of the *M* at Ring 1 of the 2 ring-model from Ring 1 of the 12 ring-model, is around 2% at Sec. 2 for k_{n} = 100 MN/m^3 under BC1 and BC2. This is because the $r_{\mathrm{M\,min}}$ is sensitive due to the fact that $\left|M_0\right|_{\max}$ is close to zero for stiff ground as shown in Figure 12.

5. CONCLUSIONS

The sectional force of the segmental lining in the cases of staggered building was analyzed by the proposed 3-D finite element model, to investigate the boundary conditions, which satisfy the quasi 2D plane strain condition, taking the boundary condition at the ring end, ground stiffness and the number of ring in the model, as parameters. As a result, the following conclusions can be made:

1) In the analysis on the sectional forces of the segmental lining with staggered building, the following model is required: 1) the full dimension of the 3D finite element model in continuum ground model, since the multi-ring model is necessary due to the non-symmetric allocation of the longitudinal joints; and 2) the quasi 2D plane strain condition.
2) The proposed model with BC1, which fixes the displacement in the tunnel axis direction only on the transverse cross section at the tunnel end, has influence of the boundary condition at the tunnel end on the sectional forces of the segmental lining, in the case of staggered building, especially in the case of axial force in soft ground.
3) The proposed model with BC2, which fixes the displacement in the tunnel axis direction and allows the rotation around the tunnel axis, on the transverse cross section at the tunnel end, can get almost demonstrate same sectional forces at the model end of the 2 ring-model and the 12 ring-model, and the center of the model of the 12 ring-model. This indicates that the proposed model with BC2 can calculate the sectional forces of the segmental lining with staggered building under quasi 2D plane strain condition, using the 2 ring-model.

6. REFERENCES

Chaiyaput, S., and Sugimoto, M. (2016) "Effect of boundary conditions in segmental lining model on its sectional force", Journal of Lowland Technology International (LTI), 18, Issues 1, pp9-22.

Dasari, G. R., Rawlings, C. G., and Bolton. M.D. (1996) "Numerical modelling of a NATM tunnel construction in London clay", Geotechnical Aspects of Underground Construction in Soft Ground, Mair and Taylor (editors), Balkema, pp491-496.

Gnilsen, R. (1989) "Underground structures: Design and instrumentation", In R. S. Sinha (Ed.), (chap. Numerical Methods). Amsterdam, Netherlands: Elsevier Science Publishers.

Huang, X., Huang, H., and Zhang, J. (2012) "Flattening of jointed shield-driven tunnel induced by longitudinal differential settlements", Tunnelling and Underground Space Technology, 31, pp20-32.

Japan Society of Civil Engineers (JSCE) (2006) "Standard Specification for Tunneling-2006: Shield Tunnels", JSCE.

Klappers, C., Grübl, F., and Ostermeier, B. (2006) "Structural analyses of segmental lining – coupled beam and spring analyses versus 3D-FEM calculations with shell elements", Proc. of World Tunnel Congress 2016. ITA.

Koyama, Y. (2003) "Present status and technology of shield tunneling method in Japan", Tunnelling Underground Space Technology, 18, pp145-159.

Li, Z., Soga, K., Bian X., and Wright, P. (2013) "Ovalisation of cast-iron bolted tunnels and their modelling", Proceedings of EURO: TUN 2013 Computational Methods in Tunneling and Subsurface Engineering, Germany.

Lu, L., Lu, X., Fan, P. (2006) "Full-ring experimental study of the lining structure of Shanghai Changjing Tunnel", Proceedings 4th International Conference on Earthquake Engineering, Oct. 12-13 Taipei, Taiwan No.056.

Muir Wood, A. M. (1975) "The circular tunnel in elastic ground", Geotechnique, Thomas Telford, London, 25, Issues 1, pp115-127.

Railway Technical Research Institute (RTRI). (2002) "Design Standards for Railway Structures and Commentary (Urban Mountain Tunnel)", RTRI. (in Japanese).

Sharma, J. S., Zhao, J., and Hefny, A.M. (2000) "NATM-Effect of shortcrete setting time and excavation sequence on surface settlements", Tunnel and Underground Structures, Zhao, Shirlaw&Krishnan (eds), Balkema, pp535-540.

Sugimoto, M., Sramoon, A., and Okazaki, M. (2011) "Tunnel lining design method by frame structure analysis using ground reaction curve". J. Japan Society of Civil Engineering, 67, Issues 1, pp61-77 (in Japanese).

Teachavorasinskun, S., and Chub-uppakarn, T. (2010) "Influence of segmental joints on tunnel lining", Tunnelling and Underground Space Technology, 25, Issues 4, pp490-494.

Yeo, C. H., Lee, F. H., Tan, S. C., Hasegawa, O., Suzuki, H., and Shinji, M. (2009) "Three dimensional numerical modelling of a NATM tunnel", International Journal of the JCRM, 5, pp33-38.